**Proceedings of the ASME 2012 International Design Engineering Technical Conferences &
Computers and Information in Engineering Conference
IDETC/CIE 2012
August 12-15, 2012, CHICAGO, USA**

DRAFT: NONLINEAR MODELING AND ANALYSIS OF ELECTROMAGNETIC BEARINGS WITH PERMANENT MAGNETS FOR BIAS

Peiman Naseradinmousavi
CENDAC
Department of Mechanical Engineering
Villanova University
Villanova, Pennsylvania 19085
Email: pnaser01@villanova.edu

C. Nataraj, Professor & Chair
CENDAC
Department of Mechanical Engineering
Villanova University
Villanova, Pennsylvania 19085
Email: nataraj@villanova.edu

Matthew V. Frank
NSWCCD
Energy Conversion R&D
Office of Naval Research
Philadelphia, Pennsylvania
Email: Matthew.Frank@navy.mil

ABSTRACT

This article describes high fidelity modeling of electromagnetic (EM) bearings with permanent magnets (PM) used to supply bias current. We analyze both the PM and EM parts of the system. Magnetic circuit theory is first used to gain insight into the magnetic forces and allows for the dynamic analysis of a rigid rotor coupled with the magnetic bearings. The results reveal that the magnetic forces are a strong nonlinear function of the rotor offsets from its equilibrium position. Next, the validity of the simplifying assumptions is examined with the aid of the finite element method. Comparisons of the magnetic forces are presented and discussed.

INTRODUCTION

Magnetic bearings support rotating machinery without physical contact, friction or wear. They require no lubrication, increase reliability, and especially reduce noise relative to conventional bearings. Magnetic bearings are also well suited to operate at higher temperatures, higher rotational speeds, and extreme altitudes, and are hence a promising solution to current limitations [1]. Magnetic bearings are increasingly being used in industrial machines such as compressors, turbines, pumps, motors, and generators. They have also been pressed into operation in ship board rotating machinery for the US Navy.

Typically, the bias current required in active magnetic bearings is produced by an electric circuit. However, the bias current could also be produced by using permanent magnets as has been proposed [2]. This invention has led to some patents as well. AVCON, Inc. initially worked with Lewis research center on the development of a magnetic bearing system for a cyrogenic magnetic bearing test facility [3]. The bearings were extensively tested over a two-year time span and those tests provided a set of data on the performance of magnetic bearings under severe conditions. In further development the permanent magnets were used to produce the main magnetic flux and the electromagnets were used to regulate the flux to control the rotor offsets. For discussion, we will call these newer types of bearings PMEM bearings and call the rather conventional electromagnetic bearings, EM bearings.

The PMEM bearings have the advantage that the power consumption is decreased and the overall size could possibly be reduced. In general, the magnetic bearings are actively controlled relative to passive bearings, and can also be designed to efficiently reduce vibration, shock response, and acoustic transmissions [4]. However the rotor dynamic analysis becomes more difficult in the presence of the coupling between the dynamics of the rotor and that of the magnetic bearings since the applied magnetic forces are highly nonlinear. Clearly, we need accurate models to be able to predict the behavior quantitatively as well as qualitatively to capture nonlinear dynamic phenomena. In particular, the analytical modeling of the PMEM bearings, as reported in the literature, is quite approximate and needs to be refined. Clearly, a refined model would increase accuracy of prediction and enhance confidence and hence enable large-scale use.

The magnetic field generated by the magnets, either electro-

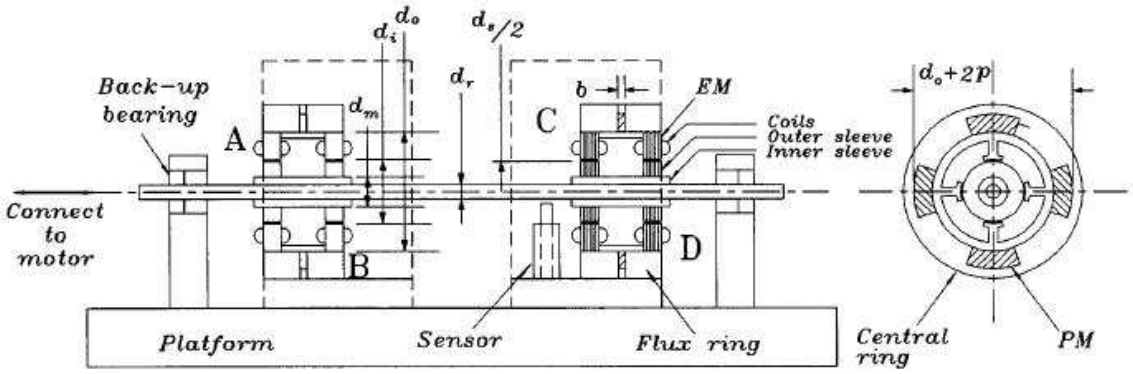

FIGURE 1. PMEM bearing model introduced by Lee, Hsiao and Kuo [2]

magnets or permanent magnets, is approximated in the literature with many assumptions including that of uniform fields, negligible fringing and leakage, and almost always ignoring the nonlinearity. Any critical ship board machinery should be capable of operating through significant shock events that may occur during wartime service or storms. The Navy specification *MIL-S-901* defines shock testing requirements for such equipment [5]. This has been a problem for many magnetic bearing supported machinery; clearly, a high fidelity magnetic model of the bearings with a good understanding of the physics should hence be developed with the highest priority prior to the applications of the exciting magnetic bearing technology on board Navy ships and other transportation vehicles subjected to large disturbance but to strict performance expectation.

The past literature is quite slim for PMEM bearings. The analytical expressions for stiffness and peak load in stacked-structure radial magnetic bearings have been presented by Paden *et al.* [6]. The asymptotic approximations to force and stiffness characteristics of magnetic bearings formed from concentric permanent magnet rings having rectangular cross sections have been done by Chen *et al.* [7]. Murakami *et al.* [8] have addressed a new energy storage flywheel system using a superconducting magnetic bearing (SMB) and a permanent magnet bearing (PMB). The magnetic vector potential has been exploited to obtain a three dimensional analytical solution for axially polarized bearings by Jiang *et al.* [9]. Ohji *et al.* [10] have reported a comparative evaluation of the permanent magnet configuration and its effects on the radial disturbance attenuation and magnetic losses. PMEM bearing modeling has been largely carried out by [2]; more discussion follows on their work.

This paper follows on the previous work done by Nataraj [4,11–13] and Frank [14]. The nonlinearity of the magnetic force and the coupling between rotor and magnetic bearings will be further addressed. A magnetic circuit approach [15, 16] is utilized to calculate the magnetic force acting on the rotor.

MATHEMATICAL MODELING

The system investigated here follows a rotor-bearing configuration developed by Lee *et al.* [2] as shown in Fig. 1. The rotor is supported by two sets of PMEM. Each PMEM includes a PM part and two EM sections. The main flux is provided by its PM part where the EM is utilized for regulating the flux.

The PM part includes four permanent magnets in a circular fashion. The stator of the EM is a four-rib stator wound by equal number of turns of control currents. The coils along each axis are connected in series and excited independently by the vertical and horizontal control currents as shown in Fig. 2.

A nonuniform distribution of the airgap flux results in a nonzero magnetic force acting on the rotor in the direction of deviation when the rotor moves from its concentric position. The EM coils are excited with the current proportional to the magnitude of deviation to control the rotor position. This results in decreasing and increasing values of the fluxes in the narrowed and widened sides of the airgap.

The PM flux flows along a loop parallel to the shaft axis where the EM flux flows along the loop normal to the shaft axis without passing through the PM.

The PMEM can be generally categorized, namely, as “coplanar” and “non-coplanar”. The PMEM modeled here is a non-coplanar type as shown in Fig. 3. The flux path determines the type of a PMEM; for a non-coplanar PMEM, the flux paths of the PM and the EM are not the same.

For simplicity, we neglect flux leakage, fringing, and eddy currents. We also assume a linear BH relation and a uniform flux distribution within the air gaps. Note that the PM material exhibits a straight demagnetization curve. Using the Ampere’s law one has,

$$\phi = BS \tag{1}$$

where,

ϕ is the magnetic flux.

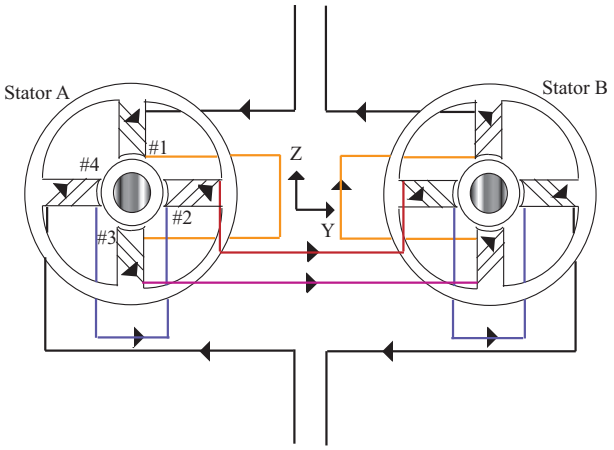

FIGURE 2. PMEM circuit configuration

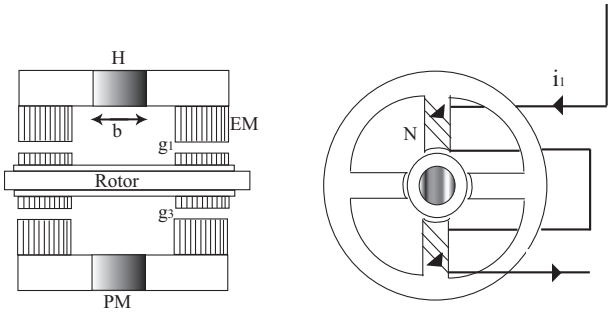

FIGURE 3. Configuration of a non-coplanar PMEM

B indicates the magnetic flux density.

S is the projected cross section area of the media normal to the flux.

By definition,

$$\phi \sum_{i=1}^{n} R = Ni \tag{2}$$

where,

N is the number of coils of the EM part.

i is the control current.

$\sum_{i=1}^{n} R$ is the path reluctance.

The simplified relation of the field intensity and the control current can be written as follows.

$$Hl = Ni \tag{3}$$

Shown in Fig. 4 is the electric circuit of the PM part. Combining Eqs. 1, 2, and 3, one finds

$$\phi \sum_{i=1}^{n} R = \frac{B_r}{\mu} \tag{4}$$

where, μ indicates the slope of the demagnetization curve of a PM material at the working point. Eq. 4 can be rewritten as follows.

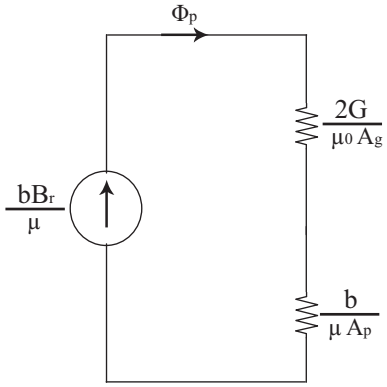

FIGURE 4. The electric circuit of the PM part

$$\phi(2R_g + R_r + R_p) = \frac{B_r}{\mu} \tag{5}$$

where,

B_r is the residual flux density of the PM part.

R_g indicates the reluctance of the air gap.

R_r related to the reluctance of the rotor.

R_p is the reluctance of the PM part.

Note that the value of the rotor reluctance is negligible in comparison with the reluctance of air gap since $\mu_r = 2000 \gg 1$. The values of R_g, for both the top and bottom air gaps, and R_p are calculated as follows.

$$R_{gt} = \frac{G - w}{\mu_0 A_g} \tag{6}$$

$$R_{gb} = \frac{G + w}{\mu_0 A_g} \tag{7}$$

$$R_p = \frac{b}{\mu A_p} \tag{8}$$

For a non-coplanar PMEM with nominal air gap of width G, the thickness of the PM in the axial direction, b, and the vertical rotor displacement, w, the magnetic flux of both the top and bottom air gaps shown in Fig. 3 are found as follows.

$$\phi_{p,1} = \frac{\mu_0 A_g A_p b B_r}{2(G-w)\mu A_p + b\mu_0 A_g} \tag{9}$$

$$\phi_{p,3} = \frac{\mu_0 A_g A_p b B_r}{2(G+w)\mu A_p + b\mu_0 A_g} \tag{10}$$

where,

μ_0 is the air permeability; $4\pi \times 10^{-7}$.

A_g is the effective area of the air gap.

A_p is the pole face area.

Shown in Fig. 5 is the electric circuit of the EM part. With respect to the loop equations for 13421, 43564, 65786, and the node equation of nodes 2468, one easily has,

$$\phi_1 = \frac{(\frac{1}{R_2} + \frac{2}{R_3} + \frac{1}{R_4})Ni_1 + (\frac{1}{R_4} - \frac{1}{R_2})Ni_2}{1 + \frac{R_1}{R_2} + \frac{R_1}{R_3} + \frac{R_1}{R_4}} \tag{11}$$

$$\phi_3 = \frac{(\frac{1}{R_2} + \frac{2}{R_1} + \frac{1}{R_4})Ni_1 + (\frac{1}{R_2} - \frac{1}{R_4})Ni_2}{1 + \frac{R_3}{R_1} + \frac{R_3}{R_2} + \frac{R_3}{R_4}} \tag{12}$$

where, R_1-R_4 indicate the reluctances of the paths. For the rotor offset along z axis, R_1-R_4 are found as follows.

$$R_2 = R_4 = R = \frac{G}{\mu_0 A_g}, R_1 = \frac{G-w}{G}R, R_3 = \frac{G+w}{G}R \tag{13}$$

Substituting Eq. 13 into Eqs. 11 and 12, the magnetic flux generated by the EM part for both the top and bottom air gaps can be found as follows.

$$\phi_{e,1} = \mu_0 A_g N i_1 \frac{2G+w}{2G^2 - w^2} \tag{14}$$

$$\phi_{e,3} = \mu_0 A_g N i_1 \frac{2G-w}{2G^2 - w^2} \tag{15}$$

With respect to Eq. 1 and the simplified relation of the magnetic force and flux density stated as follows.

$$F_{mag} = \frac{B^2 S}{2\mu_0} \tag{16}$$

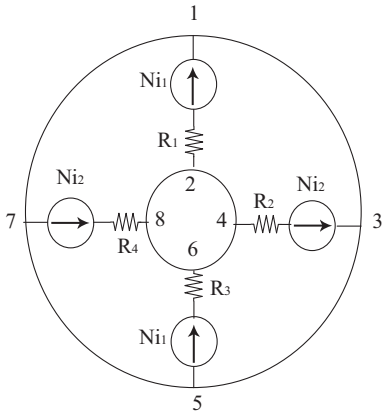

FIGURE 5. The electric circuit of the EM part

One has,

$$F_{mag} = \frac{\phi^2}{2\mu_0 S} \tag{17}$$

The vertical magnetic force of a PMEM can be calculated as follows. We name it as F_{zz} to indicate the force on the z direction due to the current i_1 in the z direction. Similarly, F_{xz} and F_{yz} stand for the forces, respectively, along x and y axes that would result from the current along the z axis.

$$F_{zz} = 2\left(\frac{\phi_1^2}{2\mu_0 A_g} - \frac{\phi_3^2}{2\mu_0 A_g}\right) \tag{18}$$

Substituting Eqs. 9, 10, 14, and 15 into Eq. 18 yields,

$$F_{zz} = \frac{1}{\mu_0 A_g}\left(\left(\frac{\mu_0 A_g A_p b B_r}{2(G-w)\mu A_p + b\mu_0 A_g} + \mu_0 A_g N i_1 \frac{2G+w}{2G^2-w^2}\right)^2 - \left(\frac{\mu_0 A_g A_p b B_r}{2(G+w)\mu A_p + b\mu_0 A_g} - \mu_0 A_g N i_1 \frac{2G-w}{2G^2-w^2}\right)^2\right) \tag{19}$$

Next, the values calculated for the magnetic force (Eq. 19) due to the rotor offset along z axis are compared to those of finite element modeling approach. Note that neglecting some nonlinearities such as flux leakage and fringing would be expected to yield smaller values of the bearing forces, in the x and y directions, generated by the rotor offset along z axis. We examine the validity of these assumptions in the next section.

FINITE ELEMENT MODELING OF PMEM BEARINGS

As stated earlier, the amount of current used for the magnetic bearing operation is greatly reduced because the bias flux

is utilized by the permanent magnets in the PMEM bearing. Figs. 6 and 7 present the finite element model of the PMEM bearing and its distribution of magnetic flux density when the rotor is in its concentric position.

Fig. 7 illustrates considerable amounts of magnetic flux density at the top air gap generated by the PM part of the PMEM. Fig. 8 exhibits a streamline plot of the magnetic flux density when the rotor has no eccentricity; note that the flux leakage and eddy currents are distinguishable within the boundary condition defined for the model. Note that we neglected these kinds of nonlinearities in our analytical model.

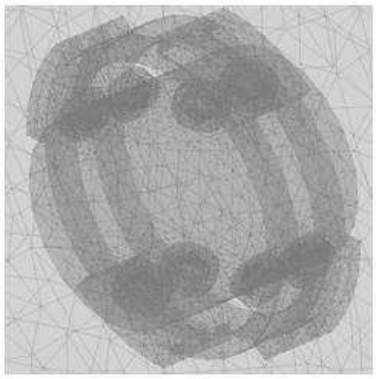

FIGURE 6. Finite element modeling of a PMEM

The geometrical and circuit parameters of the PMEM modeled are given in Table 1.

r_0: Rotor radius
r_1: Radius of pole surfaces
r_3: Inner radius of the magnetic flux rings
r_4: Outer radius of the magnetic flux rings
μ_r: Rotor and stator permeability
μ_{r-PM}: Relative permeability of permanent magnets
b: Length of the permanent magnets
A_g: Effective area of each pole surface
A_p: Effective area of permanent magnets
B_r: Residual magnetic field intensity of the permanent magnets
I_b: Current bias
I_c: Current control
G: Nominal gap size

Shown in Fig. 9 (a-d) are the magnetic flux densities of the PMEM bearing including the vertical control currents of the EM coils (see Fig. 2), $i_1 = 1,4A$, for two values of eccentricities, $w = 0.25mm$ and $w = 0.45mm$, along the z axis. The total number of degrees of freedom (DOF) considered in the FE model is $410,742$.

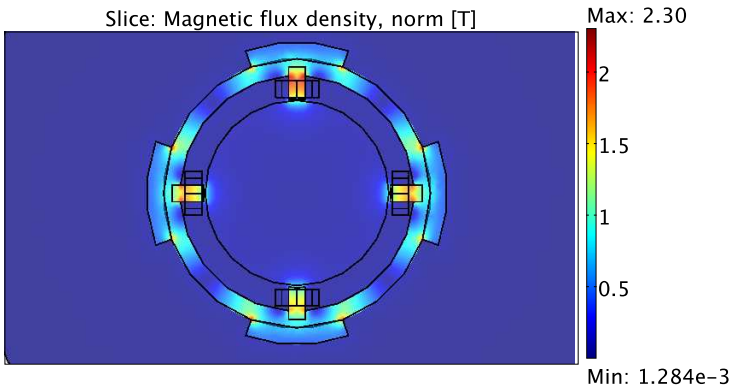

FIGURE 7. Magnetic flux density of the rotor for $w = 0mm$ and $i_1 = 1A$

Figs. 10 and 11 present the electromagnetic forces along the z axis due to the rotor offset in the same direction when the control currents show $1A$ and $4A$. The FEM result shown in Fig. 10 is somewhat similar to that of the analytical model though a spike close to the nominal maximum displacement can be distinguished probably due to the numerical issues. As would be expected, the accuracy of the analytical method seems questionable with increasing values of the control current, as shown in Fig. 11. This kind of behavior would be justified in connection with the assumptions made for neglecting the nonlinearities.

On the other hand, the nonlinearities neglected undoubtedly result in higher values of the magnetic flux density which directly affects the magnetic force generated via Eq. 16.

TABLE 1. Parametric values of the PMEM bearing

–	**PMEM**		
r_0	$27.5mm$	r_1	$28mm$
G	$0.5mm$	r_3	$35mm$
r_4	$40mm$	μ_r	$2000NA^{-2}$
μ_{r-PM}	1.05	b	$8mm$
A_g	$25.05mm^2$	A_p	$147.017mm^2$
B_r	$1.2T$	I_b	0
I_c	$1A, 4A$		

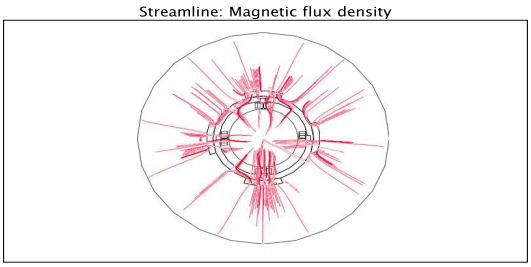

(a) 2D streamline plot of magnetic flux density

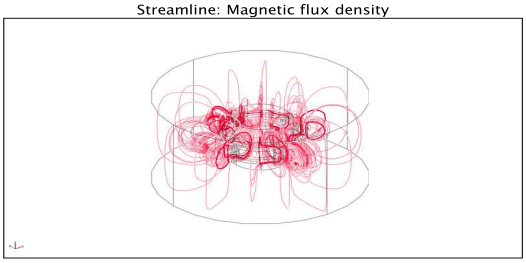

(b) 3D streamline plot of magnetic flux density

FIGURE 8. 2D and 3D streamline plots of the PMEM for $i = 1A$ and $w = 0mm$

Clearly, a nonlinear relationship exists between the magnetic force and the control current stated in Eq. 19 in the sense that increasing values of the control current, typically from $1A$ to $4A$, would yield sixteen times greater value of the magnetic force shown in Figs. 10 and 11.

Obviously, the magnetic force generated by a higher value of the control current, $4A$, is a much higher than that of a lower value of the current, $1A$, for both the approaches employed. As stated earlier, the bearing forces have been neglected by eliminating the effects of fringing, flux leakage, and other magnetic nonlinearities.

We have also investigated here the bearing forces along x and y axes that result from the vertical motion of the rotor along z axis. This is of interest to realize that our assumptions made for small values of F_{xz} and F_{yz} are valid only for small values of eccentricities.

Our calculations reveal validity of the assumptions only for values of the eccentricities limited between 0% and 50% of the rotor offset along the z axis. Under these conditions, F_{yz} can be assumed to be small in comparison with F_{zz} at the same positions of eccentricities. For example, the values of F_{yz} and F_{zz}, at 80% of the rotor offset, are $3.6423N$ and $573.98N$, respectively. Obviously, F_{yz} would take higher values by increasing values of the control currents. This is also valid for F_{xz} although the values found for F_{xz} and F_{yz} are considerably smaller than those of F_{zz}. Note that the force along x axis could be balanced by a second bearing by using a pair of bearings to control the position of the rotor.

Shown in Fig. 12 is a comparison made among the magnetic flux densities of the control currents for both the analytical and the finite element approaches. As can be seen, the analytical model loses its accuracy for higher values of the control current; we again see a spike for large displacements. Shown in Fig. 13 are the magnetic forces versus the phase angle measured from y axis when the rotor has the shown eccentricities and the control current is $1A$.

Fig. 14 shows the magnetic flux for different rotor offsets along both the y and z axes for a vertical control current of $4A$. As would be expected, the directions of the arrows change. The values of the forces are given in Table 2. Table 2 indicates a higher value of F_{yz} when the rotor has offsets along both the y and z axes than when the rotor is offset only along the z axis. This phenomenon would be explained with fact that the magnetic reluctance is reduced yielding higher values of the magnetic flux and consequently increasing the values of the magnetic force.

TABLE 2. The magnetic forces at different values of the rotor offset

–	$w = v = 0.40mm$	$w = 0.40mm, v = 0$
F_{zz}	560.93	$573.98N$
F_{yz}	$179.48N$	$3.6423N$
F_{xz}	$16.19N$	$7.3147N$

ACCURACY OF FE MODELING

In physics, a magnetic field can permeate into infinite space. However, the FE modeling for the magnetic field is limited to finite environment space. So we wish to investigate the consequence of this modeling limitation. Shown in Fig. 15 is the FE model of the PMEM bearing with different sizes of the environment space. The magnetic flux density at the middle of the top pole surface, B_g, converges from 0.966774 to 0.869475. Results show that the bigger the environment space, the more accurate magnetic flux density can be estimated. However, this leads to an increase in the degrees of freedom which creates excessive computational burden. In general, it is found that when the surrounding environment space is modeled with at least 3 times the size of PMEM bearing, an accurate magnetic flux density prediction is achieved. The FE modeling shown in Fig. 15-(b) is used for all the results related to the PMEM model in Fig. 6.

EFFECT OF SHAFT LENGTH ON MAGNETIC FLUX DENSITY

Next, we wish to investigate the effect of the shaft length on the magnetic flux density. This would give an indication of the limitations of two-dimensional modeling often adopted in magnetic bearing studies. Shown in Fig. 16 is the FE model of the PMEM bearing model for two different shaft lengths. Clearly, they result in almost the same magnetic flux density prediction. Since there are more magnetic flux losses through the shaft, the magnetic flux density at the middle of the top pole surface, B_g, is a lower value for the shown case of Fig. 16-a than that for the case in Fig. 16-b. The magnetic flux density prediction for the case with a longer shaft in Fig. 16-b is unexpectedly a little higher than that in Fig. 16-a. However, it should be noted that a coarser mesh scheme is used for the longer shaft because of memory constraints. Overall, there is little difference in the magnetic flux density prediction between the PMEM models with different shaft lengths. And thus it is not advisable to sacrifice the DOFs solved in order to adopt the whole shaft length in calculating the magnetic force on the rotor. Instead, a scale of 1 to 2 of effective shaft length to the thickness of stators would be sufficient.

CONCLUSION

In this article, some novel results of high fidelity modeling of electromagnetic bearings with permanent magnets for bias (PMEM) have been presented. The results have been compared with those of finite element analysis using COMSOL Multiphysics package. Both the analytical and FEM results indicate a strong nonlinearity of the magnetic force on the rotor offset from its equilibrium position.

The analysis using the magnetic circuit theory provides a straightforward physical insight into the magnetic forces on the rotor and hence could be applied for an initial dynamic analysis of a rigid rotor coupled with the magnetic bearings. However, the magnetic circuit approach due to some of the assumptions can be questionable in some cases. The flux leakage, fringing, and other magnetic nonlinearities show significant effects for higher values of the control current producing the magnetic flux density and consequently on the magnetic force as shown in Figs. 10 and 11. This can be attributed to the various assumptions made as discussed earlier.

To ensure accuracy in prediction, a higher fidelity FE modeling of PMEM bearings has been provided. Due to the assumptions made for the analytical approach, the bearing forces, F_{xz} and F_{yz}, have been calculated for an improved understanding of the PMEM bearing performance. Comparing with the analytical model, it is clear that assumptions stated for the bearing forces are valid only for a limited range $(0-50\%)$ of the rotor deviation from it concentric position. Note that decreasing value of the air gap results in higher values of these forces although they can still remain small to F_{zz}.

ACKNOWLEDGMENT

The senior author (CN) is grateful to the Office of Naval Research for supporting this research under Contract No. N000140710866. In particular, the efforts and guidance of Dr. Mark Spector are deeply appreciated.

REFERENCES

[1] Provenza, A. J., Montague, G. T., Jansen, M. J., and Palazzolo, A. B., 2005. "High temperature characterization of a radial magnetic nearing for turbomachinery". *Journal of Engineering for Gas Turbines Power,* ***127***(2), pp. 437–444.

[2] Lee, A. C., Hsiao, F. Z., and Ko, D., 1994. "Performance limits of permanent magnet biased magnetic bearing". *JSME International Journal,* ***37***(4), pp. 783–794.

[3] Dorf, R. C., 1992. *The electrical engineering handbook*. CRC press and IEEE press.

[4] Nataraj, C., 2005. Dynamic response of the turbocor hfc-134a centrifugal compressor rotor. Tech. rep., Office of Naval Research.

[5] Hawkins, L. A., 1997. "Shock analysis for a homopolar, permanent magnet bias magnetic bearing system". In International Gas Turbine and Aeroengine Congress and Exhibition, no. 97-GT-230.

[6] Paden, B., Groom, N., and Antaki, J. F., 2003. "Design formulas for permanent-magnet bearings". *the ASME Journal of Mechanical Design,* ***125***, pp. 734–738.

[7] Chen, C., Paden, B., Antaki, J., Ludlow, J., and Bearnson, G., 2003. "Optimal design of permanent magnet bearings with application to the heartquest ventricular assist device". *JSME International Journal,* ***46***(2), pp. 403–408.

[8] Murakami, K., Komori, M., Mitsuda, H., and Inoue, I., 2007. "Design of an enery storage flywheel system using permanent magnet bearing (pmb) and superconducting magnetic bearing (smb)". *Journal of Cyrogenics,* ***47***, pp. 272–277.

[9] Jiang, W., Allaire, P. E., Bolah, M. J., and Wood, H. G., 2002. "Stiffness analysis of axially polarized raidal permanent magnet bearings". In 8th International Symposium on Magnetic Bearing, pp. 527–532.

[10] Ohji, T., Mukhopadhyay, S., Iwahara, M., and Yamada, S., 1999. "Permanent magnet bearings for horizontal- and vertical-shaft machines: A comparative study". *Journal of Applied Physics,* ***85***, pp. 4648–4650.

[11] Nataraj, C., and Calvert, T. E., 1998. "Optimal design of radial magnetic bearings". In Proceedings of the Sixth International Symposium on Magnetic Bearings, pp. 296–305.

[12] Marx, S., and Nataraj, C., 2004. "A control technique used

to compensate for magnetic bearing responses to base motion". In ASNE EMTS Symposium.
[13] Nataraj, C., and Marx, S., 2005. "An optimal control algorithm for suppression of harmonic base excitation in nonlinear magnetic bearings". In ASME International Design Engineering Technical Conferences.
[14] Frank, M. V., 2005. "Dynamic and control analysis of a rotor supported by magnetic bearings in an air conditioning system". Master's thesis, Villanova University, May.
[15] Lee, A.-C., Hsiao, F.-Z., and Ko, D., 1994. "Analysis and testing of magnetic bearing with permanent magnets for bias". *JSME International Journal,* ***37***(4), pp. 783–794.
[16] Fan, Y.-H., and Lee, A.-C., 1997. "Design of a permanent / electromagnetic bearing-controlled system". *Journal of the Franklin Institute,* ***334B***(3), pp. 337–356.

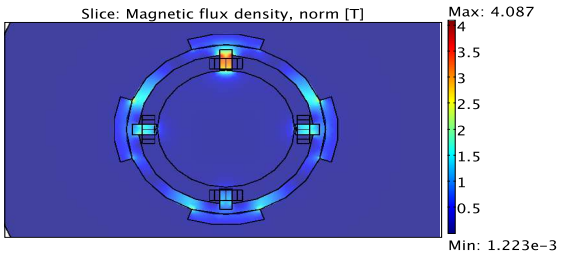

(a) $i = 1A$, $w = 0.30mm$, 60 % of the nominal gap

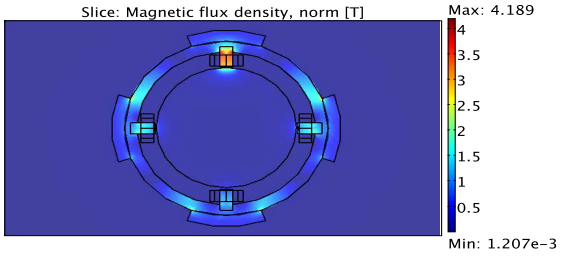

(b) $i = 4A$, $w = 0.30mm$, 60 % of the nominal gap

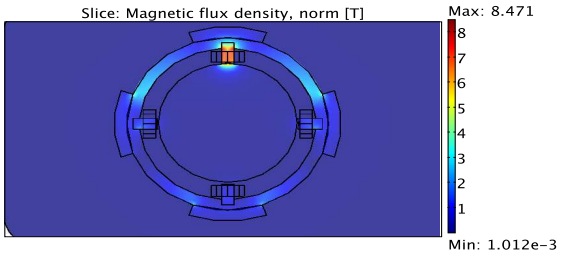

(c) $i = 1A$, $w = 0.45mm$, 90 % of the nominal gap

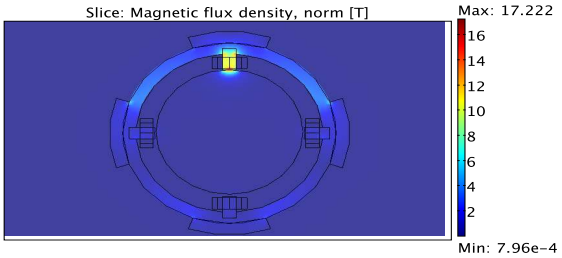

(d) $i = 4A$, $w = 0.45mm$, 90 % of the nominal gap

FIGURE 9. Magnetic flux densities for two positions of the rotor controlled by a PMEM bearing

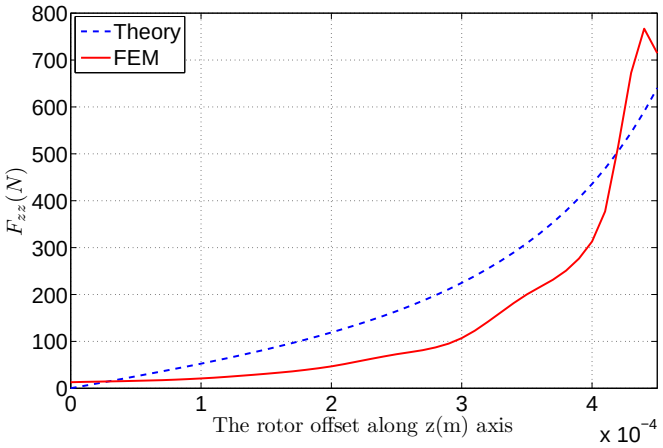

FIGURE 10. Comparison between the magnetic forces (F_{zz}) for $i_1 = 1$

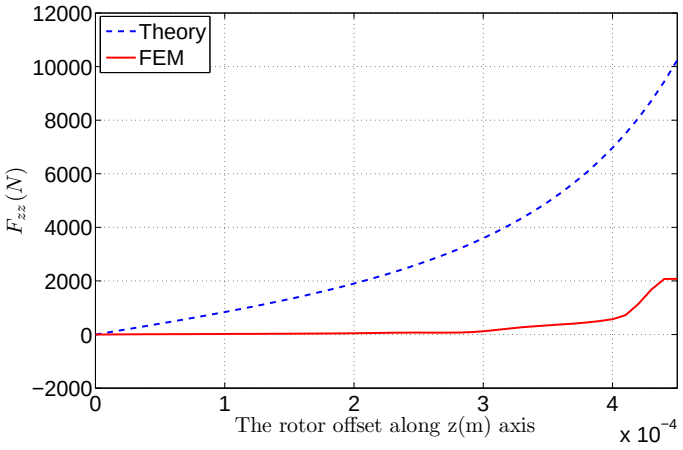

FIGURE 11. Comparison between the magnetic forces (F_{zz}) for $i_1 = 4$

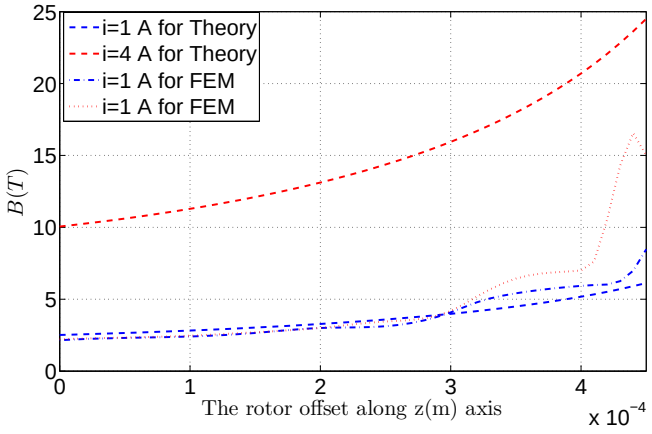

FIGURE 12. Comparison among the magnetic flux densities on the rotor offsets

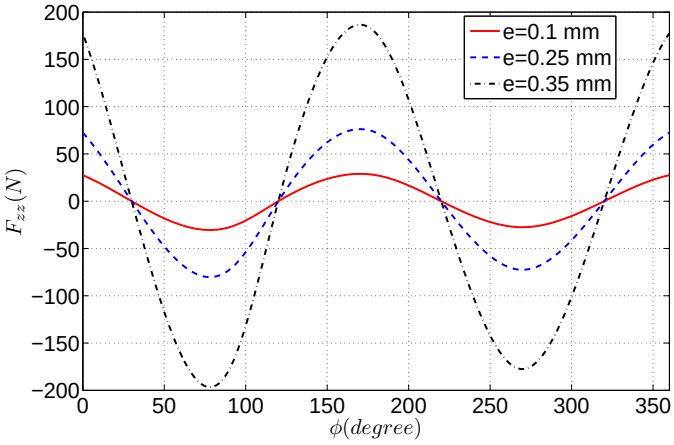

FIGURE 13. The magnetic force along y axis vs. ϕ for $e = 0.1, 0.25$, $w = 0.35mm$, and $i = 1A$

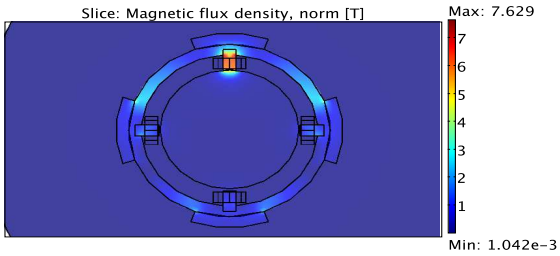

(a) $i = 4A$, $w = 0.40mm$, $v = 0$

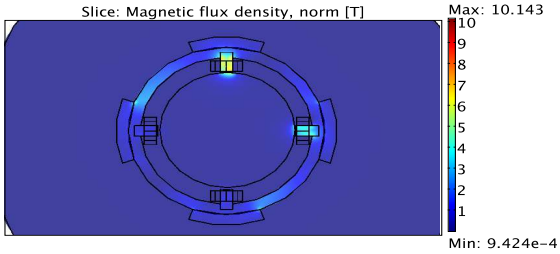

(b) $i = 4A$, $w = 0.40mm$, $v = 0.40mm$

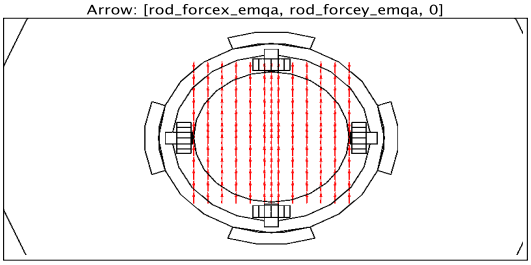

(c) Arrow plot for $i = 4A$, $w = 0.40mm$, and $v = 0mm$

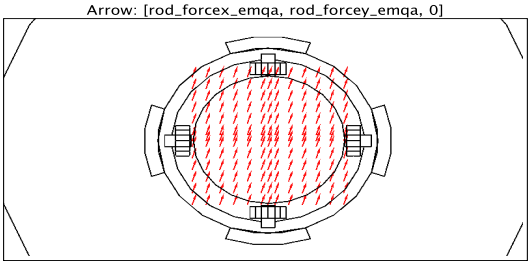

(d) Arrow plot for $i = 4A$, $w = 0.40mm$, and $v = 0.40mm$

FIGURE 14. Magnetic flux densities for the rotor offset along y and z axes

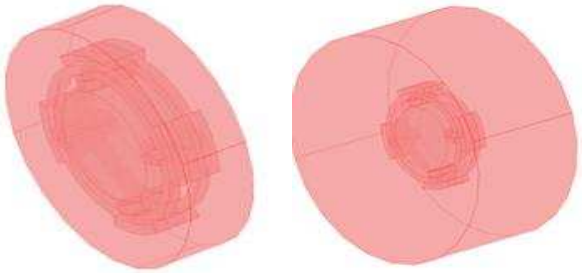

(a) $B_g = 0.966774T$ (b) $B_g = 0.873137T$

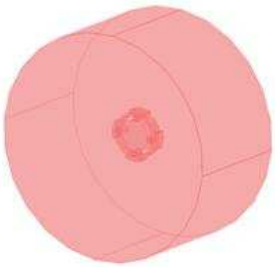

(c) $B_g = 0.869485T$

FIGURE 15. FE modeling of the PMEM bearing with increasing environment space size from (a) to (c)

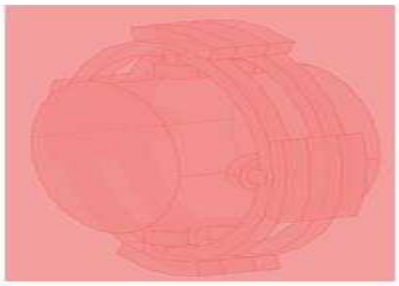

(a) $B_g = 0.843537T$

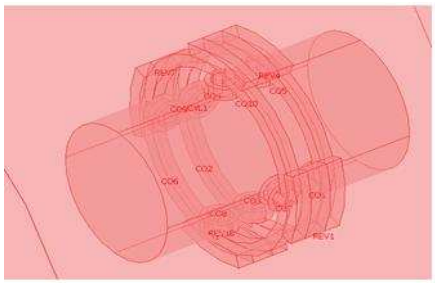

(b) $B_g = 0.845089T$

FIGURE 16. FE modeling of the PMEM bearing (a) A short shaft, and with (b) A longer shaft